A&A 662, A77 (2022)
https://doi.org/10.1051/0004-6361/202243084

Astronomy & Astrophysics

Variable mass accretion and failed wind explain changing-look phenomena in NGC 1365

S. Mondal[1], T. P. Adhikari[2], K. Hryniewicz[3], C. S. Stalin[1], and A. Pandey[1]

[1] Indian Institute of Astrophysics, II Block, Koramangala, Bangalore 560034, India
e-mail: santanuicsp@gmail.com
[2] Inter-University Centre for Astronomy and Astrophysics, Pune, Maharashtra 411007, India
e-mail: tek@iucaa.in
[3] National Centre for Nuclear Research, Ul. Pasteura 7, 02-093 Warsaw, Poland
e-mail: krzysztof.hryniewicz@ncbj.gov.pl

Received 11 January 2022 / Accepted 1 April 2022

ABSTRACT

Changing-look active galactic nuclei (CLAGNs) show a complex nature in their X-ray spectral shape and line-of-sight column-density variation. The physical mechanisms responsible for these variations are unclear. Here, we study the spectral properties of a CLAGN, NGC 1365 using combined *XMM-Newton* and *NuSTAR* observations to understand the CL behavior. The model-fitted mass-accretion rate varied between 0.003 ± 0.001 and $0.009 \pm 0.002\ \dot{M}_{\rm Edd}$ and the dynamic corona changed from 28 ± 3 to $10 \pm 1\ r_{\rm g}$. We found that the variable absorption column density correlates with the mass accretion rate and the geometry of the corona. The derived wind velocity was sufficiently low compared to the escape velocity to drive the wind away from the disc for the epochs during which column densities were high. This suggests that the high and variable absorption can be due to failed winds from the disc. Our estimated ratio of mass outflow to inflow rate from the inner region of the disc lies between 0.019 ± 0.006 and 0.12 ± 0.04. From spectral fitting of the combined data, we found the mass of the central black hole to be constant 4.38 ± 0.34–$4.51 \pm 0.29 \times 10^6\ M_{\odot}$, consistent with earlier findings. The confidence contours of $N_{\rm H}$ with other model parameters show that the model-fitted parameters are robust and non-degenerate. Our study construed that the changing accretion rate, which is a fundamental physical quantity and the geometry of the corona are driving the CL phenomena in NGC 1365. The physical picture considered in this work connects both variable continuum and variable absorbing medium scenarios.

Key words. accretion, accretion disks – black hole physics – shock waves – radiative transfer – galaxies: active – galaxies: jets

1. Introduction

An active galactic nucleus (AGN) is powered by the matter accreting onto the central supermassive black hole (SMBH) at the centre of a galaxy. The radiation coming from the accreting AGN systems shows complex features in their X-ray spectra. The components (e.g. hard, soft, or soft excess, etc.) of the spectra come from different regions within the system. A certain fraction of the hard radiation heats up the disc and generates emission lines, while a fraction is absorbed by different clouds at the line of sight (LOS). The variable absorption of the continuum coming from the central inner disc can be due to the presence of variable clouds or due to the winds from the disc.

The X-ray-absorbing column density changes dramatically by an order of magnitude over a few years in different Seyfert galaxies (Risaliti et al. 2002), which disfavours the homogeneous nature of the absorbers. Changing look (CL) AGNs are those sources that show extreme variation in the column density of the X-ray absorber, with rapid transitions between Compton-thin ($N_{\rm H} < 10^{24}\,{\rm cm}^{-2}$) and Compton-thick ($N_{\rm H} > 10^{24}\,{\rm cm}^{-2}$) regimes (e.g. Ricci et al. 2016). CLAGN though first discovered serendipitously (LaMassa et al. 2015) are now considered as a separate class of AGNs that transit from type 1 to 2 and vice versa within a timescale of decades or years (Veron et al. 1980; Maiolino & Rieke 1995; Denney et al. 2014; Yang et al. 2018; Kim et al. 2018). In Ricci et al. (2020), the CL phenomena shown for 1ES 1927+654 can be due to rapid changes in the innermost regions of accreting SMBHs.

According to models, the timescale of CL phenomenon within months or years can be due to the variation in absorbing material that appears and disappears along the LOS; this supports the quick variation in column density (Risaliti et al. 2009). On the contrary, many CLAGNs showed little variation in column density (McElroy et al. 2016; Noda & Done 2018); therefore, the CL nature could also be due to other physical processes within the system. The weak or low optical polarisation of CLAGNs suggests that the transition from type 1 to type 2 can not be attributed to the putative dust obscuration (e.g. Hutsemékers et al. 2019). The mid-infrared and optical analysis of Sheng et al. 2017 do not favour the obscuration scenario and support the notion that the CL may be caused by the intrinsic variation of accretion process. The work of Noda & Done (2018) suggests CL as a phenomenon originating from accretion processes, where radiation pressure should be significant compared to gas pressure. The radiation's pressure-driven instability is also a possible explanation for the observed timescale of CL phenomenon (Śniegowska & Czerny 2019).

NGC 1365 is a Seyfert 1.8 (Maiolino & Rieke 1995) galaxy at $z = 0.0055$ with a $10^{6.5}\ M_{\odot}$ BH (Risaliti et al. 2009). Combes et al. (2019) estimated the mass of $3.98 \times 10^6\ M_{\odot}$ from the molecular gas dynamics using ALMA data. This spiral galaxy was intensely studied by Lindblad (1999, for a review).

Article published by EDP Sciences

The source is a CLAGN due to its Compton-thin to Compton-thick transition, which can be due to variation in the LOS absorber rather than to extreme intrinsic emission variability (Matt et al. 2003; Risaliti et al. 2005). The spectral components of NGC 1365 in X-ray consists of several distinct features; for example, a Compton hump >10 keV, soft excess at low energy (below 3 keV), strong absorption features, and relativistic iron and emission lines. The source also has bi-conical outflow from the nucleus (Edmunds et al. 1988). Sandqvist et al. (1995) suggested that the AGN has a weak radio jet in this source. A [O III] line is seen in the outflow (Storchi-Bergmann & Bonatto 1991; Veilleux et al. 2003; Sharp & Bland-Hawthorn 2010). The emission lines observed for this source are dominated by collisionally ionised gas (Guainazzi et al. 2009); however, it can also be hybrid (photoionised + collisionally ionised Whewell et al. 2016, used *XMM-Newton* and *Chandra* data). NGC 1365 has some important characteristics, when it is observed in the Compton-thin state, its X-ray spectrum shows the presence of strong absorption lines due to Fe XXV (both the He-α and He-β) and Fe XXVI (both the Lyα and Lyβ components); these lines are blueshifted by $v \sim 3000\,\mathrm{km\,s^{-1}}$ (Risaliti et al. 2005; Brenneman et al. 2013). These features may have originated due to the presence of highly ionised outflowing wind and from the accretion disc. All these features are occasionally observed in Seyfert galaxies; however, it is unlikely to see all of them in a single source. Later, Connolly et al. (2014) examined that the long-term variability of the X-ray absorber could have originated from the changes in the mass-accretion rate of NGC 1365. The analysis of the *Suzaku* observation of the source suggested the presence of a partial covering and ionised absorber using photoionisation models (Gofford et al. 2013, 2015). Braito et al. (2014) evidenced that two ionised absorbers were needed to fit the RGS spectra of *XMM-Newton* and detected a possible P-Cygni profile of the Mg XII Lyα, line which is associated with a mildly ionised absorber indicative of a wide-angle outflowing wind. At the same time, Nardini et al. (2015) used the *Chandra* data to estimate the location of the photoionised gas based on some evidence of broadening of the emission lines. The central active nucleus is surrounded by a molecular torus with both narrow and broad emission line components in the emitted spectrum and relativistic iron line (Risaliti et al. 2009). The variable absorbing medium along the LOS was observed by (Rivers et al. 2015) using combined *XMM-Newton* and *NuSTAR* data. The relativistic line feature estimates the maximal spin of the BH > 0.97 (Walton et al. 2014). Kara et al. (2015) estimated soft lag due to the presence of an eclipsing cloud along the line of sight using *NuSTAR* observations. The star formation and gas accretion to the central object were studied using near-infrared (NIR) data by Fazeli et al. (2019) and Gao et al. (2021) to check for more recent star formation activities and outflow structure of the source.

Despite the source having been studied extensively in different energy bands, understanding of CL phenomena is still lacking due to little physical information being collected in earlier studies. Most of them phenomenologically explained that the variable column density is due to the appearance or disappearance of some clouds along the LOS, and none of the previous studies self-consistently considered the accretion-ejection scenario to take into account the CL phenomena. Therefore, in this work, we aim to address these phenomena after estimating fundamental physical quantities of accretion; such as mass accretion rate, corona geometry etc., considering beforehand the observational characteristics such as Compton hump, jets, winds, and variable continuum in NGC 1365 system. For that, we used joint *XMM-Newton* and *NuSTAR* data from 2012 and 2013. This paper is organised as follows: in Sect. 2, we explain the observations and data reduction procedures, and in Sect. 3, we discuss the modelling, various analyses, and data fitting carried out using different models. A brief conclusion is given in the final section.

Table 1. Log of observations. Here, X = 6000204600, and Y = 0692840 are the initials of the observation IDs.

NuSTAR	Exp. (ks)	*XMM-Newton*	Exp. (ks)	Epoch	Date	MJD
X3	41	Y201	118	A	2012-07-26	56134
X5	66	Y301	108	B	2012-12-24	56285
X7	74	Y401	93	C	2013-01-23	56315
X9	70	Y501	116	D	2013-02-12	56335

2. Observation and data analysis

We used joint *XMM-Newton* and *NuSTAR* (Harrison et al. 2013) observations of NGC 1365 during 2012 and 2013. The observation log is given in Table 1.

To analyse the *XMM-Newton* data, we used the Science Analysis System (SAS) version 19.1.0 and followed the standard procedures given in the SAS data analysis threads[1]. We first reprocessed the Observation Data Files (ODF) using the EPPROC routine to generate the calibrated and concatenated event lists. We filtered the concatenated event lists to remove the periods of high background activity. We then extracted the source and background spectra using the EVSELECT routine. We used a circular region with a radius of 32″ for both the source and the background. The background region was in the same CCD but away from the contamination of the point sources. We used RMFGEN and ARFGEN tasks to generate the redistribution matrices (.rmf) and the ancillary (.arf) files. Finally, we rebinned the spectra using the task SPECGROUP in order to have at least 25 counts in each bin.

The *NuSTAR* data were extracted using the standard NUSTARDAS version 1.3.1[2] software. We ran a NUPIPELINE task to produce cleaned event lists and NUPRODUCTS to generate the spectra. We used a region of 80″ for the source and 100″ for the background using DS9. The data were grouped by *grppha* command, with a minimum of 30 counts in each bin. For the analysis of each epoch of observation, we used the data of both *XMM-Newton* and *NuSTAR* in the energy range of 0.5−75 keV.

We used XSPEC[3] (Arnaud 1996) version 12.11.0 for spectral analysis. Each epoch of observation was fitted using an accretion-disc-based two component advective flow (TCAF Chakrabarti & Titarchuk 1995) model including a jet (JeTCAF Mondal & Chakrabarti 2021). The present model takes into account the radiation processes at the base of the jet, discussed later in detail. We used the absorption model TBABS (Wilms et al. 2000) for the Galactic absorption, keeping the hydrogen column density fixed to $1.3 \times 10^{22}\,\mathrm{cm^{-2}}$ (Kalberla et al. 2005) during the fitting. We used chi-square statistics for the goodness of the fitting. We employed source redshift here and left $N_{\rm H}$ as a free parameter to estimate the absorbing column density responsible for the overall spectral distortion.

[1] https://www.cosmos.esa.int/web/xmm-newton/sas-threads
[2] https://heasarc.gsfc.nasa.gov/docs/nustar/analysis/
[3] https://heasarc.gsfc.nasa.gov/xanadu/xspec/

3. Modelling

For the spectral fitting, we used the accretion-ejection based JeTCAF model (Mondal & Chakrabarti 2021) along with multiplicative models for instance partial covering fraction absorption (ZPCFABS) and Gaussian absorption line (GABS). The JeTCAF model geometry and flow configuration is illustrated in Fig. 1. In this model, the accretion disc has two components, one is a Keplerian disc sitting at the equatorial plane, which is the source of soft photons, and a sub-Keplerian halo (hot component) sitting above and below the Keplerian disc. The second component forms the shock in the accretion disc (Chakrabarti 1989) after satisfying Rankine-Hugoniot conditions. This shocked region behaves as the centrifugal pressure supported boundary layer (CENBOL) of the corona. The same region is also producing thermally driven jets. Matter falling into the black hole piles up inside the shocked (post-shock) region. The JeTCAF model takes into account the radiation mechanisms at the base of the jet and the bulk motion effect by the outflowing jet on the emitted spectra. This model requires six parameters (if the mass is considered as a free parameter), which are (i) the mass of the BH ($M_{\rm BH}$), (ii) the disc accretion rate ($\dot{m}_{\rm d}$), (iii) the halo accretion rate ($\dot{m}_{\rm h}$), (iv) the size of the dynamic corona or the location of the shock ($X_{\rm s}$ in $r_{\rm g} = 2GM_{\rm BH}/c^2$ unit), (v) the shock compression ratio (R), and (vi) the ratio of the solid angle subtended by the outflow to the inflow ($f_{\rm col} = \Theta_{\rm o}/\Theta_{\rm in}$).

The emergent spectrum from JeTCAF has four components; (1) a multicolour black-body spectrum coming from the disc, (2) hard radiation from the upscattering of the soft photons from the disc by the hot corona, (3) a second hard component at the shoulder of the black-body bump is due to scattering of soft photons from the disc by the base of the jet, and (4) downscattering of hard radiation from the corona by the bulk motion of the jet produces excess above 10 keV (Titarchuk & Shrader 2005; Mondal & Chakrabarti 2021). This component also fits the Compton humps that are observed in reflection models. The current JeTCAF model is an updated version (including jet) of the TCAF model, which has been successfully applied to low-mass black hole X-ray binaries (Debnath et al. 2014; Mondal et al. 2014a; Mondal & Chakrabarti 2019, and references therein) and to AGNs (e.g. Nandi et al. 2019; Mondal & Stalin 2021) to fit their spectra and to infer the underlying accretion dynamics. In this model, the same corona, which is producing hard radiation, is also launching a jet at its base. The jet/mass outflow rate becomes clear after solving a series of coupled hydrodynamic equations; thus, it naturally connects the disc and jet. As NGC 1365 evidenced the presence of both accretion discs, jets and outflows, and a Compton hump >10 keV, it is worth applying the JeTCAF model to study the CL phenomena. For the first time, we appled the JeTCAF model as a physical model to understand the CL phenomena, and we believe it has the potential to explore the observed accretion-ejection features in NGC 1365. We note that, the present model does not include detailed line emission or absorption properties.

The spectrum of NGC 1365 showed complex features including distortions from 3 to 7 keV, which can be due to a varying absorber covering the source that substantially changes the shape of the spectrum below 10 keV (Risaliti et al. 2009). It also showed broadening of the Fe line ∼6 keV in combined *XMM-Newton* and *NuSTAR* data due to relativistic effects near the inner region of the disc (Risaliti et al. 2013). Below ∼3 keV energy, the *XMM-Newton* data showed diffuse thermal contribution and significant excess below ∼2 keV, the origin of which is not yet clear. However, it may have originated via the upscattering of seed photons from the disc by a warm, optically thick medium (see for recent study Mehdipour et al. 2022, and references therein). The current JeTCAF model does not include relativistic effects; therefore, for the skewing and broadening of the Fe line shapes near the innermost region of the disc, we used the GAUSS model to take into account those effects. Furthermore, we focused on the accretion parameters and the geometrical configuration of the corona that generate variable emission, which can be successfully obtained by analysing the combined *XMM-Newton* and *NuSTAR* data in the 0.4−75 keV range. In this range, all spectra showed both emission and absorption features, those are taken into account by GAUSS and GABS models. One Gaussian component is used at ∼6.4 keV for the FeK line and the second one is used at ∼0.8 keV to fit the broad line feature at low energy. The other two/three Gaussian components are applied at different energy regions throughout the spectra; however, all are used below 6 keV. The origin of (soft) Gaussian components below 2 keV is not clear yet, however, it may have originated from distant reflection (Baloković et al. 2018). The ZPCFABS model is used for addressing the source's intrinsic absorption and partial covering and to estimate the column density along the LOS. The complete model reads in XSPEC as TBABS*ZPCFABS*GABS[2]*(GAUSS[4–5]+JeTCAF).

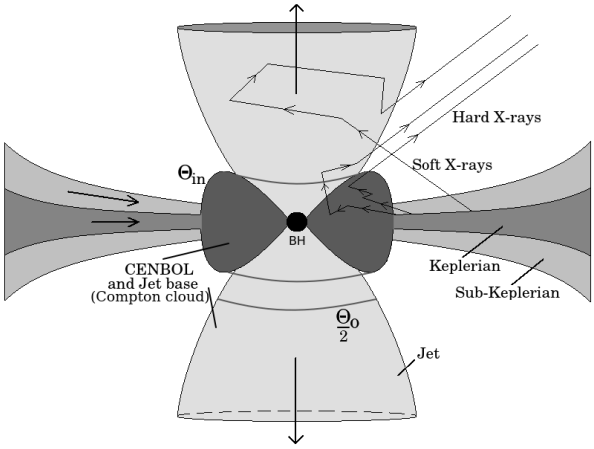

Fig. 1. Illustration of JeTCAF model. The zig-zag arrows show the scattering of photons from the disc and jet. The $\Theta_{\rm o}$ and $\Theta_{\rm in}$ are the solid angle subtended by the outflow and inflow. The figure is adopted from Mondal & Chakrabarti (2021).

The ZPCFABS model is not a good representation for an ionising medium as it does not include the effects of ionisation when generating the emission or absorption lines. For the ionisation rate estimation, freely available photoionisation software (for example CLOUDY or XSTAR, etc.) can be appropriate, as extensively discussed in the literature (see Gofford et al. 2013, 2015; Braito et al. 2014, and references therein). However, the current paper aims to quantify the accretion-ejection parameters assuming that the accretion rate and corona properties might be triggering CL phenomena; therefore, detailed ionisation modelling is beyond the scope of the paper.

4. Results and discussions

Figure 2 shows the spectral fitting to the data for four epochs. In all the spectra, we found complex features including absorption lines, skewing of the FeK line, soft excess, and some excess at high energies, which can be due to the bulk motion of the outflowing material from the central region or to reflection

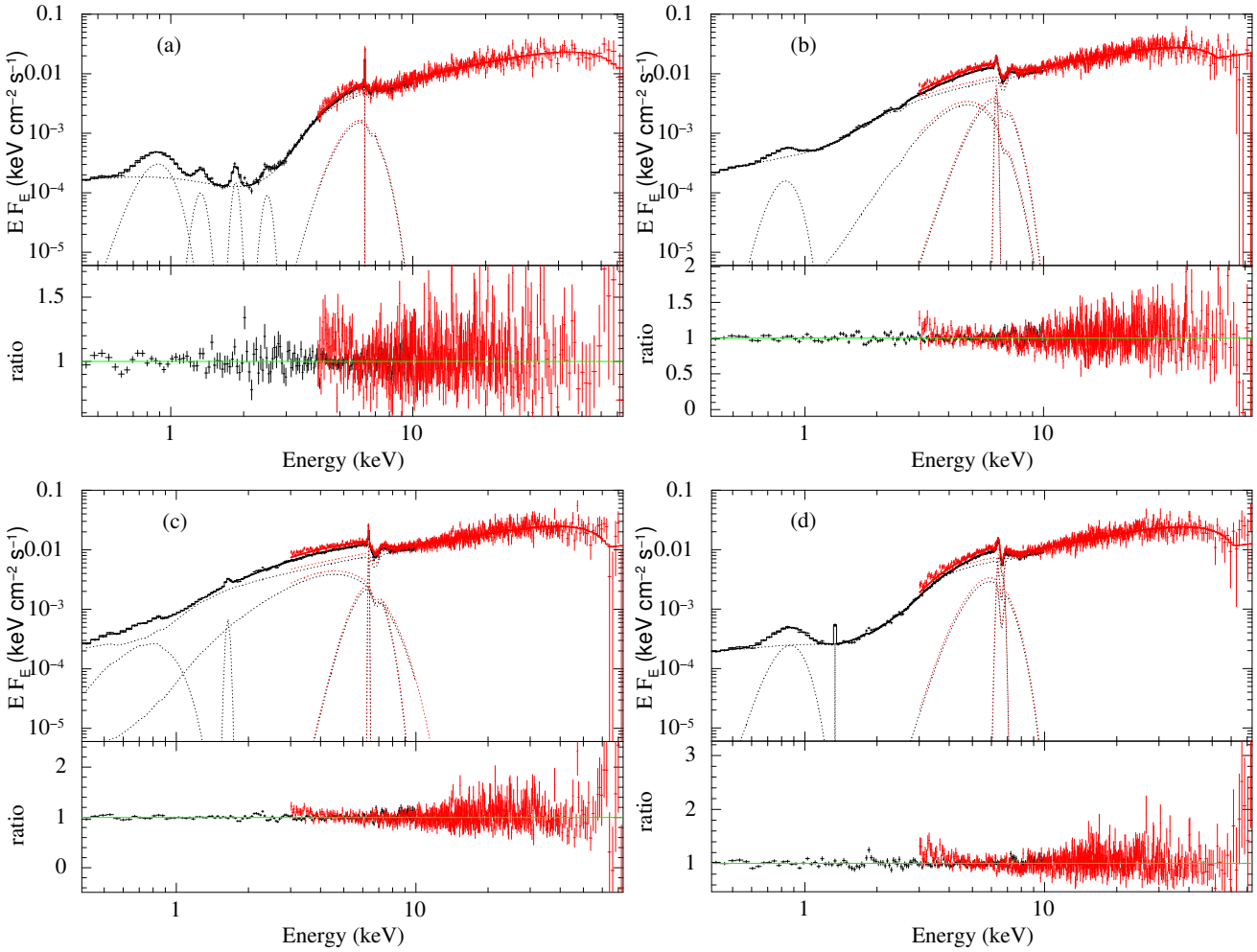

Fig. 2. `JeTCAF` model-fitted 0.4−75.0 keV spectra for all four epochs of NGC 1365 during *XMM-Newton* and *NuSTAR* era. Here, *panels a–d* corresponds to epochs A to D. The different Gaussian lines are used for emission/excess at different energy ranges, including at ∼6.4 keV. The model fits show the absorption line and spectral shape change in each epoch, along with a P Cygni profile in the FeK band.

Table 2. Best-fitted model parameters are provided in this table.

Epoch	$M_{\rm BH}$ ($\times10^6\,M_\odot$)	$\dot{m}_{\rm d}$ ($M_{\rm Edd}$)	$\dot{m}_{\rm h}$ ($M_{\rm Edd}$)	$X_{\rm s}$ ($r_{\rm g}$)	R	$f_{\rm col}$	$N_{\rm H}$ ($\times10^{22}$ cm^{-2})	$c_{\rm f}$	$E_{\rm a}^1$ (keV)	$\sigma_{\rm a}^1$ (keV)	$E_{\rm a}^2$ (keV)	$\sigma_{\rm a}^2$ (keV)	$\chi^2_{\rm r}$/d.o.f.
A	4.45 ± 0.21	0.003 ± 0.001	0.381 ± 0.028	27.8 ± 3.1	4.80 ± 0.52	0.39 ± 0.08	19.72 ± 2.27	0.79 ± 0.17	2.04 ± 0.12	0.91 ± 0.13	6.71 ± 0.08	0.17 ± 0.06	641/506
B	4.38 ± 0.34	0.007 ± 0.001	0.643 ± 0.034	14.3 ± 1.9	6.21 ± 0.51	0.22 ± 0.03	2.38 ± 0.15	0.77 ± 0.03	2.50 ± 0.02	0.11 ± 0.03	6.78 ± 0.02	0.19 ± 0.02	1101/704
C	4.48 ± 0.52	0.009 ± 0.002	0.609 ± 0.022	9.8 ± 1.2	3.91 ± 0.42	0.38 ± 0.11	0.80 ± 0.18	0.89 ± 0.08	1.87 ± 0.06	1.74 ± 0.07	6.76 ± 0.02	0.21 ± 0.03	1214/707
D	4.51 ± 0.29	0.006 ± 0.001	0.484 ± 0.024	12.7 ± 1.6	4.67 ± 0.38	0.40 ± 0.09	4.13 ± 0.67	0.87 ± 0.04	2.26 ± 0.15	0.75 ± 0.10	6.62 ± 0.15	0.12 ± 0.19	959/688

Notes. $N_{\rm H}$ and $c_{\rm f}$ are hydrogen column density and dimensionless covering fraction. $E_{\rm a}$ and $\sigma_{\rm a}$ are the absorption line energy and width. The superscripts 1 and 2 correspond to the absorption line 1 and 2.

(as reported by Rivers et al. 2015 and references therein). The model-fitted parameters are given in Table 2. The variation of the `JeTCAF` model-fitted parameters are shown in Fig. 4. The top panel shows the variation of mass, which is constant during the observation period, as expected; however, other parameters changed significantly from the second from top to bottom panels. The disc or Keplerian accretion rate was ≤1% of the Eddington rate; however, it changed significantly between epochs A to D (second panel). Braito et al. (2014) estimated the mass accretion rate for this source, which is a factor of a few higher than our estimates. It can be due to either strong dependence of their estimates on the ionised winds and the covering factor they used in their model or due to the higher mass of the BH ($10^7\,M_\odot$) used and a different accretion efficiency (0.06). The low-angular-momentum, hot-flow rate was always higher than the Keplerian one. We also noticed that the size of the dynamic corona shrunk from 28 to 10 $r_{\rm g}$. The size of the corona was changed significantly, and the disc accretion rate was low compared to the halo accretion rate; hence, these are indications of a hard/intermediate spectral state, if the spectra of an AGN allow a similar classification as that in low-mass black hole binaries. Our model-fitted shock compression ratio (R) varies between 3.9 and 6.2. As the presence of the jet confirmed from the [O III] line that the source has bi-conical outflows (Edmunds et al. 1988), we therefore estimated the mass outflow/inflow rate (dimensionless quantity) using the relation

$R_{\dot{m}} = \frac{\dot{M}_{\rm out}}{\dot{M}_{\rm tot}} = f_{\rm col} f_0^{3/2} \frac{R}{4} \exp\left[\frac{3}{2} - f_0\right]$, where $f_0 = \frac{R^2}{R-1}$ (Chakrabarti 1999), $\dot{M}_{\rm tot} = (\dot{m}_{\rm d} + R \times \dot{m}_{\rm h})$ (Mondal et al. 2014b), and $\dot{M}_{\rm out}$ is the mass outflow rate in $M_\odot\,{\rm yr}^{-1}$, respectively. The $f_{\rm col}$ value varied between 0.22 and 0.4 (Col. 7 in Table 2). Our calculated values lie in the range between 0.019 ± 0.006 and 0.12 ± 0.04. This gives a mass outflow rate of ∼0.047 $M_\odot\,{\rm yr}^{-1}$, which is in agreement (∼0.067 $M_\odot\,{\rm yr}^{-1}$) with the independent optical and *Chandra* imaging studies (Venturi et al. 2018) and the *XMM-Newton*-RGS data analysis (Braito et al. 2014).

Treating BH mass as a free parameter in `JeTCAF`, we found that the BH mass is constant (see Fig. 4) during the combined XMM and *NuSTAR* data fitting, resulting in 4.38 ± 0.34−4.51 ± 0.29 × 10^6 $M_\odot$, which closely matches (4.47 × 10^6 $M_\odot$) with the estimation by Onori et al. (2017) and the molecular gas dynamics (3.98 × 10^6 $M_\odot$) using ALMA data by Combes et al. (2019).

In addition to accretion disc parameters, the `ZPCFABS` model-fitted $N_{\rm H}$ varied (in Col. 8 of Table 2) by more than an order of magnitude from epochs A to C, and the partial covering fraction ($c_{\rm f}$) was relatively high (see Col. 9) in all four epochs; however, it was constant within the error bar. The variation of $N_{\rm H}$ with `JeTCAF` model parameters are shown in Fig. 5. The left panel shows its variation with $\dot{m}_{\rm d}$. A similar variation is observed with the halo rate and accretion rate ratio (ARR = disc rate/halo rate). This relative ratio of accretion rates is an indicator of the ratio of disc and coronal flux contribution. As the ratio is always <1, a dominant hot-flow-rate contribution is implied; thus, the radiation coming from the corona is hard. It is quite certain that changing the geometry and accretion flow properties can change the intensity of the radiation being emitted from the corona, since it reprocesses photons from the underlying accretion flow. This radiation when falling onto the disc can also influence the disc-mass outflow; thus, the column density, is shown in other panels of Fig. 5. The confidence contours of $N_{\rm H}$ with the `JeTCAF` model parameters are shown in Fig. 3 of Sect. 4.1, which show that the parameters are non-degenerate and robust.

4.1. Robustness of model parameters

Figure 3 shows the confidence contours of $N_{\rm H}$ with other `JeTCAF` model parameters. We used the steppar command in XSPEC to generate these plots. Different model parameters are labelled on the x-axis. Three different contour colours (red, green, and blue) correspond to one, two, and three sigma confidence levels. It is also the same as $\Delta\chi^2$ fit statistics of 2.3, 4.61, and 9.21. The correlation of $N_{\rm H}$ with model parameters are clearly visible from the contour plots. The uncertainty of $N_{\rm H}$ fits within 0.6 dex for a 2-sigma confidence level. The other parameters assess better precision. The correlations are clear, showing that there is no obvious degeneracy between parameters and that the solution is robust.

The top panel shows a direct correlation of $N_{\rm H}$ with $M_{\rm BH}$, $\dot{m}_{\rm d}$, and $\dot{m}_{\rm h}$, implying that if these parameter values increase, continuum luminosity will also increase; therefore, continuum-driven wind will also contain more material along the LOS. However, in the case of $X_{\rm s}$ parameter, it is the opposite. It anti-correlates with the disc accretion rate. In the case of R (up to the strong shock condition value, which is 4; see Chakrabarti 1999) and $f_{\rm col}$, increase in both the parameters, the luminosity contribution from the jet increases, and therefore the wind material launching along the LOS will increase. This gives a positive correlation. We note that in the case of $f_{\rm col}$, the contour is not closed at its higher value side (the upper limit of the grid value for this parameter is 0.5), this can be an artefact. Our continuum-driven, wind-launching correlation study agrees with the work by Gofford et al. (2015, and references therein), where the authors studied the (anti)correlation of continuum luminosity with different physical quantities of the wind applicable for a large sample.

As an additional test, we used photoionisation simulation to predict absorption and emission line spectra for the modelled intrinsic spectral energy distributions (SEDs) shown in Fig. 6. The SED includes both the disc (UV/optical photons), corona, and jet component (hard X-ray) as discussed in Sect. 3. In the `JeTCAF` model, we computed the EUV photons considering the disc to be multi-temperature at each radius. At the zeroth iteration, the flux emitted from the disc is purely Keplerian (Shakura & Sunyaev 1973). These seed photons are upscattered by the hot corona. As the iterations go on, the interception of corona photons by the disc is taken into consideration, which modifies the original disc temperature. In order to estimate the transmitted spectrum that an observer can measure along the LOS, we performed the numerical simulation of radiation transfer using the photoionisation code CLOUDY17.02 (Ferland et al. 2017). The essential parameters, the SED, gas density $n_{\rm H}$, and column density $N_{\rm H}$ are adopted in such a way that satisfies the spectral fitting from Table 2. The illuminating SEDs used in CLOUDY are the `JeTCAF` model components from Fig. 2 fitted for each epoch (excluding the other components). The gas density values $n_{\rm H}$ = 2.65 × 10^{10}, 1.73 × 10^{11}, 1.47 × 10^{11}, and 1.01 × 10^{11} cm^{-3} are taken for epochs A to D, respectively. Likewise, the column density values, $N_{\rm H}$ = 1.97 × 10^{23}, 2.38 × 10^{22}, 0.8 × 10^{22}, and 4.13 × 10^{22} cm^{-2} are adopted from Col. 8 of Table 2 for epochs A to D, respectively. The models are computed for the two representative cases of the ionisation parameters ξ = 10^2 and 10^3 erg cm s^{-1}, respectively. The $N_{\rm H}$ and ξ values fall within the range estimated in the literature (Gofford et al. 2013; Walton et al. 2014; Braito et al. 2014 and references therein). The $N_{\rm H}$ values presently obtained are approximated values, as the fit does not consider ionisation effects to the continuum. In all of these simulations, we considered the solar values of the chemical composition, which are defaults in CLOUDY adopted from Grevesse & Sauval (1998). In order to account for the effects of micro-turbulence in absorption-emission lines, typical turbulent velocity of $v_{\rm turb}$ = 1000 km s^{-1} is used. Here, we did not estimate or quantify the turbulent velocity but considered a typical value as a test case to generate the observed lines; however, for a detailed study for this effect, we refer the reader to Gofford et al. (2013). We note that only the classical approach of one-dimensional radiation transfer with plane-parallel open geometry without the inclusion of relativistic effects were considered. For the details of CLOUDY applications in various AGN environments and generic definitions of parameters used, we refer the reader to the relevant literature (see Adhikari et al. 2015, 2019; Adhikari 2019) and cloudy documentation *Hazy* files[4].

We provide a zoomed-in view of the transmitted spectra for bands at 6−9 keV in Fig. 7. The results from CLOUDY simulations show absorption in the region around 6.4 keV, which is similar to that seen in the observed spectra shown in Fig. 2. The change in the spectral shapes, reflected in the illuminating SEDs in CLOUDY, during the transition from epoch A to epoch D also changes the extent of Fe absorption. For the lowest value of mass accretion rate (0.003 $\dot{M}_{\rm Edd}$) in epoch A, there is a considerable amount of Fe absorption, and it becomes weak as the accretion

[4] https://gitlab.nublado.org/cloudy/cloudy/-/wikis/home

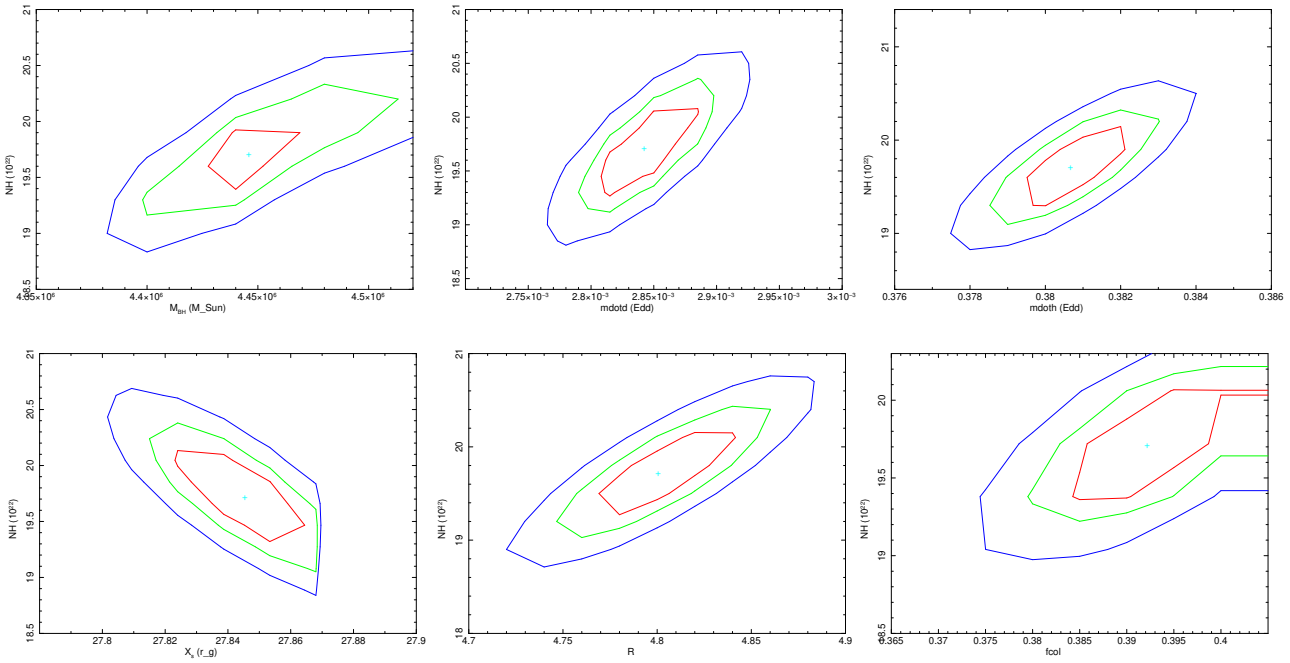

Fig. 3. Confidence contour of $N_{\rm H}$ with different continuum model parameters for epoch A. Three different contour colours show the confidence level of one (red), two (green), and three sigma (blue). Here, x labels follow the parameter notations used in Table 2; that is mdotd, mdoth, and fcol represent $\dot{m}_{\rm d}$, $\dot{m}_{\rm h}$, and $f_{\rm col}$, respectively.

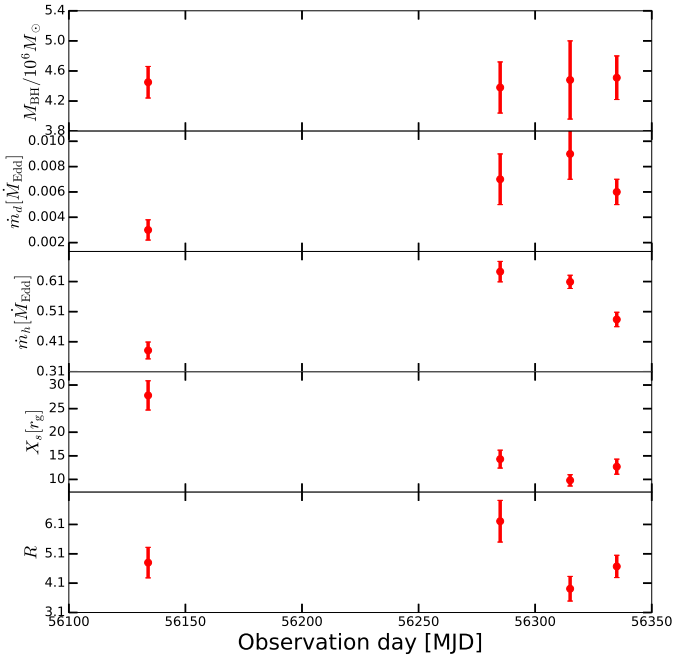

Fig. 4. Variation of JeTCAF model-fitted parameters with observational epochs.

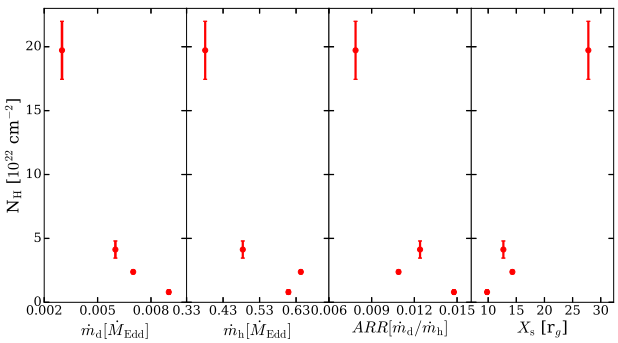

Fig. 5. $N_{\rm H}$ decreases with increasing accretion rates, and an opposite profile is observed with the geometry of the corona.

rate reaches its maximum (0.009 $\dot{M}_{\rm Edd}$) in epoch C. This result from basic simulations in CLOUDY nicely corroborates with the observed features of absorption presented in Fig. 2. However, the emission lines observed are somehow skewed or broadened by the general relativistic (GR) effects of the highly spinning source. These effects are not included in CLOUDY spectra, and thus several components of narrow emission lines are present in Fig. 7. We noticed that the energy at which the absorption is significant depends on the adopted value of the ξ in the photoionisation models. The increase in ξ allows for the ionisation of Fe to higher levels and as a result significant absorption towards the higher energy bands are seen. We note that this CLOUDY modelling was done to check whether the model SEDs for a given ionisation parameter and turbulent velocity can generate emission and absorption lines similar to what is or not observed for NGC 1365. However, this approach does not measure the ξ parameter robustly, it requires a detailed study. We plan to address this issue with a grid of photoionisation simulations and ionisation parameter variations in the future work.

4.2. Failed wind scenario

We consider here the case of the absorber is being associated with the outflowing matter. One of the most prominent outflowing regions within AGNs is the broad line region (BLR); it is also one of the candidates hosting intervening matter. Studies of warm absorbers (WA) observed at X-rays consider disc

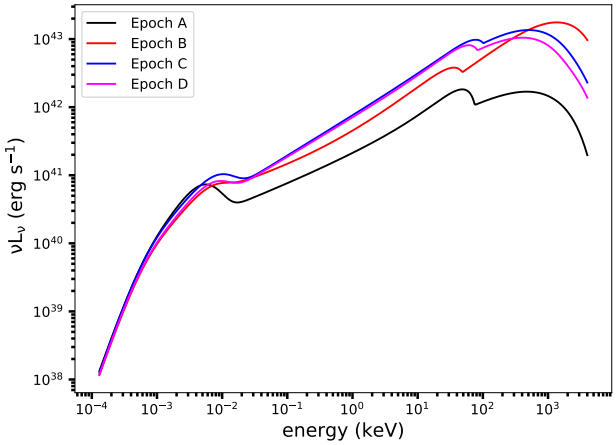

Fig. 6. The incident SEDs used in CLOUDY models for the four epochs considered here. The SEDs are computed using the `JeTCAF` model which includes relevant physical processes in the accretion disc. The EUV flux is computed assuming the disc is emitting modified multi-color blackbody photons from each radius of the disc.

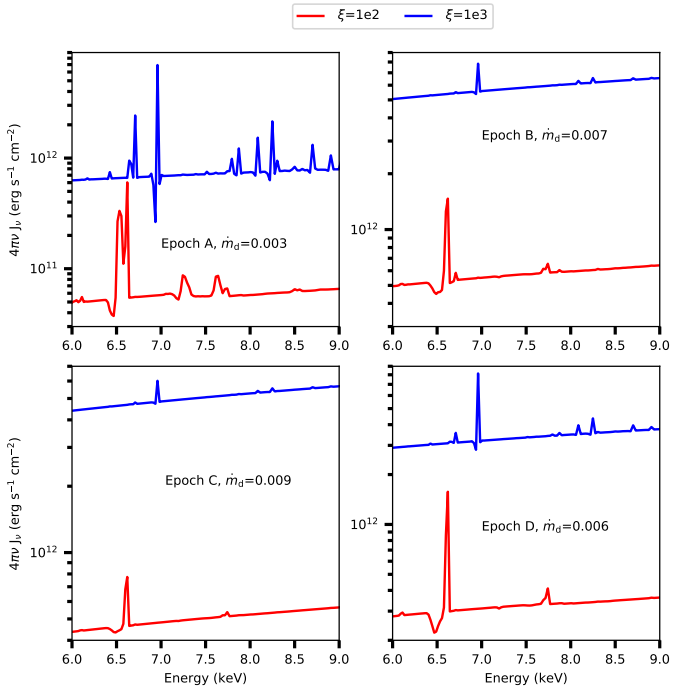

Fig. 7. Zoomed-in view of the simulated spectra zoomed between 6 and 9 keV for four different epochs using CLOUDY photoionisation code. The evolution of the absorption properties with the change in the disc mass-accretion rates (as seen from the fitted data) are plotted in each panel. The red and blue lines correspond to $\xi = 100$ and 1000, respectively. The micro-turbulence of $v_{\rm turb} = 1000\,{\rm km\,s^{-1}}$ is used in the simulations for all epochs.

outflow or the BLR as a source of absorption (Maiolino et al. 2010; Risaliti et al. 2011), or at least one of its components (like NGC 5548 case described by Kaastra et al. 2014). Also, torus can be responsible for part of the absorption (Mrk 509 study by Kaastra et al. 2012). The expected ionisation parameter value suggested here, $\log\xi \sim 2{-}3$, agrees with the values expected at the BLR position. Thus, we give theoretical consideration to the BLR-like outflow. One of the possible outflow scenarios is the failed radiatively driven outflow (FRADO) model, which clearly connects the BLR with the underlying accretion disc (Czerny & Hryniewicz 2011).

We assume that the wind moves away from the disc with constant speed, $v_{\rm w}$, in the form of a partial, thin, spherical shell at a distance of $R_{\rm BLR}$ from the central source. The amount of mass per unit time carried out by the wind is

$$\dot{M}_{\rm w} = \mu m_{\rm p} N_{\rm H} v_{\rm w} R_{\rm BLR} \Omega, \tag{1}$$

where $\mu = 1.4$, $m_{\rm p} = 1.67 \times 10^{-24}$ gm, $\Omega = \pi/2$ (Maiolino & Rieke 1995), and $R_{\rm BLR}$ are the mean atomic mass per proton, proton mass, typical value of the solid angle subtended by the outflow, and the radius of the BLR, respectively. From our spectral fitting, we found that $N_{\rm H}$ decreases with increasing $\dot{m}_{\rm d}$ and follows the relation $\mathcal{N}\dot{m}_{\rm d}^{-\beta}$. For NGC 1365, $\mathcal{N} \sim 1.5 \times 10^{17}\,{\rm cm^{-2}}$ and β, and 2.43 ± 0.15.

To estimate the radial position of the outflowing matter, we used an empirical relation based on reverberation mapping results for nearby AGNs (i.e. Bentz et al. 2009), which is supported and explained by the FRADO model. The BLR radius can be estimated from the following solution of Czerny & Hryniewicz (2011):

$$\log R_{\rm BLR} = 1.538 \pm 0.027 + 0.5 \log L_{44,5100} \tag{2}$$

where $R_{\rm BLR}$ is in light days and $L_{44,5100}$ is the monochromatic luminosity at 5100 Å (λL_λ) measured in units of $10^{44}\,{\rm erg\,s^{-1}}$. We can translate $L_{44,5100}$ to the bolometric luminosity using the relation $L_{\rm bol} = 10.33\,L_{5100}$ (Richards et al. 2006). The $L_{\rm bol}$ is calculated using the relation $\eta\dot{m}_{\rm d}c^2$, where $\eta = 0.1$ is considered. Our estimated values for $R_{\rm BLR}$ (in cm) using Eq. (2) are $\{3.61 \times 10^{15}, 5.47 \times 10^{15}, 6.27 \times 10^{15}$, and $5.14 \times 10^{15}\}$ for epochs A to D and are consistent with the literature.

As the radiation from the central region falls onto the wind, and considering that on average each emitted photon scatters about once before escaping to infinity, this suggests that the total wind momentum must be of the order of the photon momentum (King 2010). This can be written as

$$\dot{M}_{\rm w} v_{\rm w} \simeq \frac{L_{\rm bol}}{c}, \tag{3}$$

where c is the speed of light.

After solving a few steps, we find the equation for the wind velocity to be

$$v_{\rm w} = \frac{L_{\rm bol}^{0.5}\dot{m}_{\rm d}^{\beta/2}}{(\mathcal{N} c m_{\rm p} R_{\rm BLR} \mu\Omega)^{1/2}} = 30\left(\frac{L_{\rm bol}\dot{m}_{\rm d}^{\beta}}{\mathcal{N} R_{\rm BLR}}\right)^{1/2} {\rm km\,s^{-1}}. \tag{4}$$

Our estimated wind velocities for all four epochs from A to D are 1445, 4978, 7235, and 4001 km s^{-1}, respectively. The estimated wind velocities fall in the range reported in earlier studies on continuum-driven wind launching (see Gofford et al. 2013, 2015; Braito et al. 2014, and references therein). In epochs A and D, the velocity values are less than the wind terminal velocity's attained maximum (5748 and 4839 km s^{-1} estimated using $\sqrt{2GM_{\rm BH}/R_{\rm BLR}}$; here, G = gravitational constant). For epoch B, the wind velocity is comparable with its wind terminal velocity (4623 km s^{-1}). This failed wind behaves as a cloud shielding the central emission. However, in epoch C, wind velocity higher than the terminal velocity (4365 km s^{-1}) can help to drive the material away from the disc; therefore, much less column density was observed. A similar scenario was studied earlier for a low-mass black hole binaries (Miller et al. 2020).

From the model fits, we see the high-absorption, variable column density along the LOS, which we argue could be due to the failed wind above the disc surface. The disc accretion rate was low, implying the radiative pressure was also low, and therefore the wind launched from the disc could stay in place and the matter was not pushed by the radiation to outer radii. In addition, strong ionising radiation or outflows (which is often observed in the hard or intermediate spectral states when the accretion rate is low) from the central region of the disc itself can over-ionise the wind from the disc, which can prevent the wind from being driven away from the disc, and therefore its velocity decreases (for an extensive study in Proga & Kallman 2004). On the other hand, the failed wind BLR model suggests that the outflow velocity scales with the accretion rate. This happens because of its strong connection with the underlying accretion disc. The dusty matter is pushed away from the disc atmosphere by the radiation from the underlying disc and is later exposed to the central radiation, which breaks its driving force or pushes it more forcefully to the outer radii (Naddaf et al. 2021). There are other physical mechanisms that can produce different emission/absorption lines in an AGN environment, as was recently discussed in Laha et al. (2021, for a review).

5. Conclusions

In this work, we studied the CLAGN NGC 1365 using an accretion-ejection model including absorption and line emission in order to understand the maximum possible underlying physical processes behind this CL phenomenon. From our analysis, we provide the following conclusions.

- The accretion rates and their ratio, and the size of the dynamic corona, varied significantly during the observation period.
- The compression ratio of the shock at the boundary layer of the dynamic corona lies between 3.9 and 6.2, which is used to estimate the mass outflow rate from the dynamic corona. The maximum outflow rate estimated is ∼12% of the inflow rate. This confirms the previous findings that the outflows are present in the system.
- The geometry/size of the dynamic corona is also responsible for variable luminosity, which correlates with the hydrogen column density along the LOS.
- The accretion-ejection model-fitted mass is placed within a range between $4.38 \pm 0.34 - 4.51 \pm 0.29 \times 10^6\, M_\odot$ and, remarkably, matches with the estimation by Onori et al. (2017).
- The presence of prominent absorption line and high hydrogen column density is due to a low mass-accretion rate. The low accretion rate is not able to generate enough pressure to push the matter farther out from the disc (consistent with recent simulation by Naddaf et al. 2021); therefore, it blocks the radiation coming from the inner region. This is also evidenced from the CLOUDY simulations, where absorption features are stronger (at the highest $N_{\rm H}$) for the low mass-accretion state. This explains the 'failed wind' scenario due to low wind velocity.
- We studied the correlation between $N_{\rm H}$ with other model-fitted continuum parameters (see Sect. 4.1) and found that they are consistent with the physical picture of the model and agree with the earlier works on continuum driven wind launching (Gofford et al. 2015 and references therein).

Therefore, CLAGNs can show significant variability if the accretion rate and the corona geometry change substantially. We also describe the physical origin of CL phenomena using these basic flow parameters.

Acknowledgements. We thank the referee for helpful comments and suggestions that improved the quality of the manuscript. S.M. acknowledges funding from Ramanujan Fellowship grant (# RJF/2020/000113) by SERB-DST, Govt. of India. T.P.A. gratefully acknowledges the Inter-University Center for Astronomy and Astrophysics (IUCAA), Pune, India for providing the access to the Computational Cluster, where the numerical simulations used in this paper are performed. This research has made use of the *NuSTAR* Data Analysis Software (NUSTARDAS) jointly developed by the ASI Science Data Center (ASDC), Italy and the California Institute of Technology (Caltech), USA. This research has also made use of data obtained through the High Energy Astrophysics Science Archive Research Center Online Service, provided by NASA/Goddard Space Flight Center.

References

Adhikari, T. P. 2019, Photoionization Modelling as a Density Diagnostic of Line Emitting/Absorbing Regions in Active Galactic Nuclei (Cham: Springer International Publishing)
Adhikari, T. P., Różańska, A., Sobolewska, M., & Czerny, B. 2015, ApJ, 815, 83
Adhikari, T. P., Różańska, A., Hryniewicz, K., Czerny, B., & Behar, E. 2019, ApJ, 881, 78
Arnaud, K. A. 1996, in XSPEC: The First Ten Years, eds. G. H. Jacoby, & J. Barnes, ASP Conf. Ser., 101, 17
Baloković, M., Brightman, M., Harrison, F. A., et al. 2018, ApJ, 854, 42
Bentz, M. C., Peterson, B. M., Netzer, H., Pogge, R. W., & Vestergaard, M. 2009, ApJ, 697, 160
Braito, V., Reeves, J. N., Gofford, J., et al. 2014, ApJ, 795, 87
Brenneman, L. W., Risaliti, G., Elvis, M., & Nardini, E. 2013, MNRAS, 429, 2662
Chakrabarti, S. K. 1989, ApJ, 347, 365
Chakrabarti, S. K. 1999, A&A, 351, 185
Chakrabarti, S., & Titarchuk, L. G. 1995, ApJ, 455, 623
Combes, F., García-Burillo, S., Audibert, A., et al. 2019, A&A, 623, A79
Connolly, S. D., McHardy, I. M., & Dwelly, T. 2014, MNRAS, 440, 3503
Czerny, B., & Hryniewicz, K. 2011, A&A, 525, L8
Debnath, D., Chakrabarti, S. K., & Mondal, S. 2014, MNRAS, 440, L121
Denney, K. D., De Rosa, G., Croxall, K., et al. 2014, ApJ, 796, 134
Edmunds, M. G., Taylor, K., & Turtle, A. J. 1988, MNRAS, 234, 155
Fazeli, N., Busch, G., Valencia-S., M., et al. 2019, A&A, 622, A128
Ferland, G. J., Chatzikos, M., Guzmán, F., et al. 2017, Rev. Mex. Astron. Astrofis., 53, 385
Gao, Y., Egusa, F., Liu, G., et al. 2021, ApJ, 913, 139
Gofford, J., Reeves, J. N., Tombesi, F., et al. 2013, MNRAS, 430, 60
Gofford, J., Reeves, J. N., McLaughlin, D. E., et al. 2015, MNRAS, 451, 4169
Grevesse, N., & Sauval, A. J. 1998, Space Sci. Rev., 85, 161
Guainazzi, M., Risaliti, G., Nucita, A., et al. 2009, A&A, 505, 589
Harrison, F. A., Craig, W. W., Christensen, F. E., et al. 2013, ApJ, 770, 103
Hutsemékers, D., Agís González, B., Marin, F., et al. 2019, A&A, 625, A54
Kaastra, J. S., Detmers, R. G., Mehdipour, M., et al. 2012, A&A, 539, A117
Kaastra, J. S., Kriss, G. A., Cappi, M., et al. 2014, Science, 345, 64
Kalberla, P. M. W., Burton, W. B., Hartmann, D., et al. 2005, A&A, 440, 775
Kara, E., Zoghbi, A., Marinucci, A., et al. 2015, MNRAS, 446, 737
Kim, D. C., Yoon, I., & Evans, A. S. 2018, ApJ, 861, 51
King, A. R. 2010, MNRAS, 402, 1516
Laha, S., Reynolds, C. S., Reeves, J., et al. 2021, Nat. Astron., 5, 13
LaMassa, S. M., Cales, S., Moran, E. C., et al. 2015, ApJ, 800, 144
Lindblad, P. O. 1999, A&ARv, 9, 221
Maiolino, R., & Rieke, G. H. 1995, ApJ, 454, 95
Maiolino, R., Risaliti, G., Salvati, M., et al. 2010, A&A, 517, A47
Matt, G., Guainazzi, M., & Maiolino, R. 2003, MNRAS, 342, 422
McElroy, R. E., Husemann, B., Croom, S. M., et al. 2016, A&A, 593, L8
Mehdipour, M., Kriss, G. A., Brenneman, L. W., et al. 2022, ApJ, 925, 84
Miller, J. M., Zoghbi, A., Raymond, J., et al. 2020, ApJ, 904, 30
Mondal, S., & Chakrabarti, S. K. 2019, MNRAS, 483, 1178
Mondal, S., & Chakrabarti, S. K. 2021, ApJ, 920, 41
Mondal, S., & Stalin, C. S. 2021, Galaxies, 9, 21
Mondal, S., Debnath, D., & Chakrabarti, S. K. 2014a, ApJ, 786, 4
Mondal, S., Chakrabarti, S. K., & Debnath, D. 2014b, Ap&SS, 353, 223
Naddaf, M.-H., Czerny, B., & Szczerba, R. 2021, ApJ, 920, 30
Nandi, P., Chakrabarti, S. K., & Mondal, S. 2019, ApJ, 877, 65
Nardini, E., Gofford, J., Reeves, J. N., et al. 2015, MNRAS, 453, 2558

Noda, H., & Done, C. 2018, MNRAS, 480, 3898
Onori, F., Ricci, F., La Franca, F., et al. 2017, MNRAS, 468, L97
Proga, D., & Kallman, T. R. 2004, ApJ, 616, 688
Ricci, C., Bauer, F. E., Arevalo, P., et al. 2016, ApJ, 820, 5
Ricci, C., Kara, E., Loewenstein, M., et al. 2020, ApJ, 898, L1
Richards, G. T., Lacy, M., Storrie-Lombardi, L. J., et al. 2006, ApJS, 166, 470
Risaliti, G., Elvis, M., & Nicastro, F. 2002, ApJ, 571, 234
Risaliti, G., Elvis, M., Fabbiano, G., Baldi, A., & Zezas, A. 2005, ApJ, 623, L93
Risaliti, G., Miniutti, G., Elvis, M., et al. 2009, ApJ, 696, 160
Risaliti, G., Nardini, E., Salvati, M., et al. 2011, MNRAS, 410, 1027
Risaliti, G., Harrison, F. A., Madsen, K. K., et al. 2013, Nature, 494, 449
Rivers, E., Risaliti, G., Walton, D. J., et al. 2015, ApJ, 804, 107
Sandqvist, A., Joersaeter, S., & Lindblad, P. O. 1995, A&A, 295, 585
Shakura, N. I., & Sunyaev, R. A. 1973, A&A, 24, 337
Sharp, R. G., & Bland-Hawthorn, J. 2010, ApJ, 711, 818
Sheng, Z., Wang, T., Jiang, N., et al. 2017, ApJ, 846, L7
Śniegowska, M., & Czerny, B. 2019, ArXiv e-prints [arXiv:1904.06767]
Storchi-Bergmann, T., & Bonatto, C. J. 1991, MNRAS, 250, 138
Titarchuk, L., & Shrader, C. 2005, ApJ, 623, 362
Veilleux, S., Shopbell, P. L., Rupke, D. S., Bland-Hawthorn, J., & Cecil, G. 2003, AJ, 126, 2185
Venturi, G., Nardini, E., Marconi, A., et al. 2018, A&A, 619, A74
Veron, P., Lindblad, P. O., Zuiderwijk, E. J., Veron, M. P., & Adam, G. 1980, A&A, 87, 245
Walton, D. J., Risaliti, G., Harrison, F. A., et al. 2014, ApJ, 788, 76
Whewell, M., Branduardi-Raymont, G., & Page, M. J. 2016, A&A, 595, A85
Wilms, J., Allen, A., & McCray, R. 2000, ApJ, 542, 914
Yang, Q., Wu, X.-B., Fan, X., et al. 2018, ApJ, 862, 109